RSC Advances

PAPER

View Article Online
View Journal | View Issue

Cite this: *RSC Adv.*, 2021, **11**, 30315

New quinoxaline-based VEGFR-2 inhibitors: design, synthesis, and antiproliferative evaluation with *in silico* docking, ADMET, toxicity, and DFT studies†

Mohammed M. Alanazi,[a] Hazem Elkady,[*b] Nawaf A. Alsaif,[a] Ahmad J. Obaidullah,[a] Hamad M. Alkahtani,[a] Manal M. Alanazi,[a] Madhawi A. Alharbi,[a] Ibrahim H. Eissa[*b] and Mohammed A. Dahab[*b]

A new series of 3-methylquinoxaline-based derivatives having the same essential pharmacophoric features as VEGFR-2 inhibitors have been synthesized and evaluated for their antiproliferative activities against two human cancer cell lines, MCF-7 and HepG-2. Compounds **15b** and **17b** demonstrated a significant antiproliferative effect with IC_{50} ranging from 2.3 to 5.8 μM. An enzymatic assay was carried out for all the tested candidates against VEGFR-2. Compound **17b** was the most potent VEGFR-2 inhibitor (IC_{50} = 2.7 nM). Mechanistic investigation including cell cycle arrest and apoptosis was performed for compound **17b** against HepG-2 cells, and the results revealed that **17b** induced cell apoptosis and arrested cell cycle in the G2/M phase. Moreover, apoptosis analyses were conducted for compound **17b** to evaluate its apoptotic potential. The results showed upregulation in caspase-3 and caspase-9 levels, and improving the Bax/Bcl-2 ratio by more than 10-fold. Docking studies were performed to determine the possible interaction with the VEGFR-2 active site. Further docking studies were carried out for compound **17b** against cytochrome P450 to present such compounds as non-inhibitors. *In silico* ADMET, toxicity, and physico-chemical properties revealed that most of the synthesized members have acceptable values of drug-likeness. Finally, DFT studies were carried out to calculate the thermodynamic, molecular orbital and electrostatic potential properties.

Received 4th August 2021
Accepted 30th August 2021

DOI: 10.1039/d1ra05925d

rsc.li/rsc-advances

1. Introduction

Deregulation of the cell cycle may cause cancer onset, progression, and metastasis.[1,2] Receptor tyrosine kinases (RTKs) play a central role in cellular proliferation.[3] RTK expression is highly organized in normal cells; however, in cancer cells overexpression of some RTKs was observed.[4] Similarly, the vascular endothelial growth factor receptor (VEGFR), an important RTK, plays a remarkable role in angiogenesis.[5] It is composed of three isoforms, VEGFR-1, VEGFR-2 and VEGFR-3.[6] Chiefly, VEGFR-2 is the main mediator of angiogenesis in cancer cells.[7] Signaling of VEGFR-2 is up-regulated at specific phases of cancer to support tumor proliferation and expansion.[8] The main concept to discover novel VEGFR-2 inhibitors is to hinder autophosphorylation and dimerization processes of the receptor.[9]

Small molecule inhibitors targeting the kinase domain (KD) leading to blocking signaling pathway hence, suppression of tumor growth.[10] In 2007, sorafenib **I** turned into the first VEGFR-2 inhibitor[11] to be utilized in the treatment of hepatocellular carcinoma and renal cell carcinoma.[12] During the previous few decades, several VEGFR-2 inhibitors were designed as an adjunctive for cancer therapy. Regorafenib **II**,[13] lenvatinib **III**,[14] cabozantinib **IV**,[15] tivozanib **V**,[16] and sunitinib **VI**[17] were marketed for the treatment of different types of cancers (Fig. 1).

VEGFR-2 inhibitors are classified into three classes: (i) ATP competitive inhibitors, binds to the zone which is fitted by adenine ring of ATP *e.g.* sunitinib.[18] (ii) Inhibitors that are not able to bind at adenine binding site but bind beside the hydrophobic pocket *e.g.* sorafenib.[18] (iii) Covalent inhibitors which covalently bind to cysteine amino acid residue at the binding site and hinder binding of ATP *e.g.* vatalanib.[19]

Quinoxaline derivatives are a widespread class of the heterocycles receiving the most attention especially in the field of chemotherapy.[20–22] Many drugs incorporating quinoxaline moiety achieved promising results and have been submitted to clinical trials for anticancer therapeutic purposes.[23,24]

In this work, some quinoxaline derivatives were synthesized and evaluated for their cytotoxicity and VEGFR-2 inhibitory activity. The most active candidate was assessed for its

[a]*Department of Pharmaceutical Chemistry, College of Pharmacy, King Saud University, P.O. Box 2457, Riyadh 11541, Saudi Arabia*

[b]*Pharmaceutical Medicinal Chemistry & Drug Design Department, Faculty of Pharmacy (Boys), Al-Azhar University, Cairo 11884, Egypt. E-mail: mohammeddahab@azhar.edu.eg; ibrahimeissa@azhar.edu.eg; Hazemelkady@azhar.edu.eg*

† Electronic supplementary information (ESI) available. See DOI: 10.1039/d1ra05925d

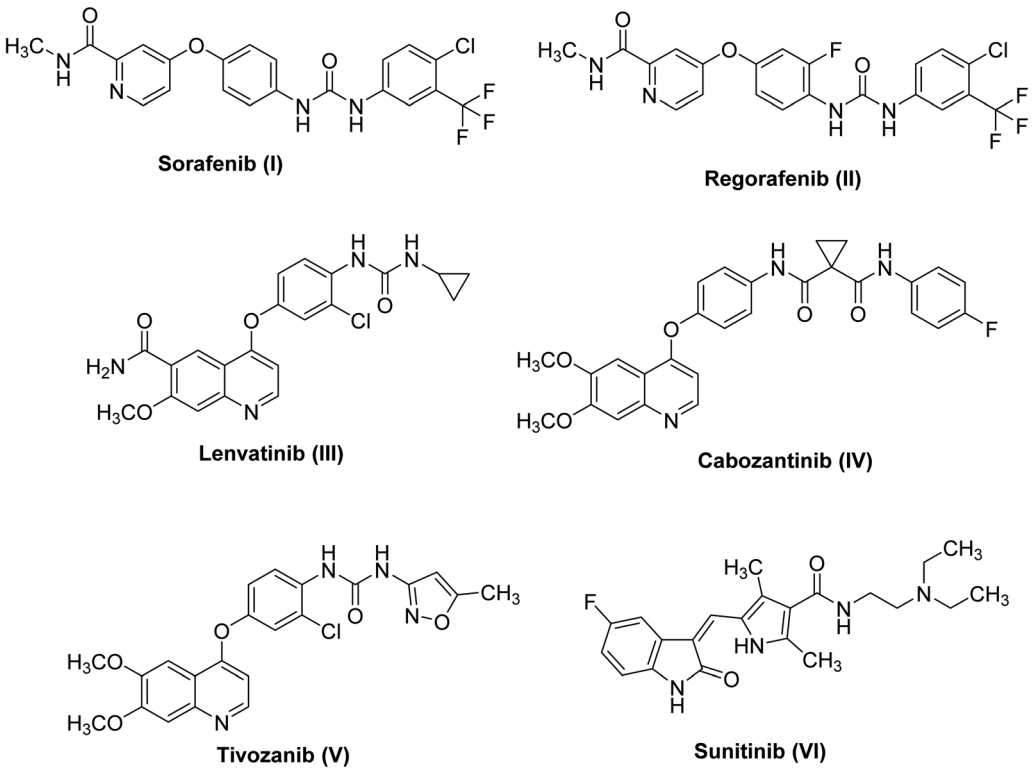

Fig. 1 Chemical structures of some FDA-approved VEGFR-2 inhibitors.

apoptotic effect and cell cycle arrest. Different *in silico* docking studies were carried out to predict the binding interaction with the prospective target (VEGFR-2) *via* docking studies. Also, *in silico* ADMET and toxicity studies were performed to predict the level of drug likeness. Furthermore, DFT studies were carried out to predict the HOMO and LUMO energy as well electrostatic potential map.

1.1 Design concept

Based on the above-mentioned findings and in the extension of our former work targeting anticancer derivatives,[25–32] especially VEGFR-2 inhibitors[33,34] we synthesized new quinoxaline derivatives as based on the study of the structure–activity relationships (SAR) of different VEGFR-2 inhibitors. VEGFR-2 inhibitors were found to share basic pharmacophoric features. (i) A head group which is required to be flat hetero aromatic to occupy the hinge region (colored green in Fig. 2). (ii) A hydrophobic spacer to occupy the linker area between the ATP binding domain and the DFG domain of the enzyme[35] (colored purple in Fig. 2). (iii) A hydrogen-bonding (pharmacophore) moiety that is required to achieve hydrogen bond interactions with Asp1044 and Glu883 in the DFG motif[36] (colored red in Fig. 2). (iv) A terminal hydrophobic (tail) moiety which occupies the allosteric hydrophobic back pocket[37] (colored blue in Fig. 2).

The main concept of our design was achieved by bioisosteric alteration of VEGFR-2 inhibitors (sorafenib & sunitinib). Such modifications were done at four positions. Firstly, bioisosteric replacement of pyridine or indole rings by 3-methylquinoxalin-2(1*H*)-one or 3-methylquinoxaline-2-thiol moieties in the hinge region to occupy the adenine region in the ATP binding pocket. The second strategy was to use *N*-phenylacetamide moiety in the spacer region instead of the central aryl ring of the lead structures aiming to improve VEGFR-2 binding affinity. Thirdly, we noticed that the conserved hydrogen-bonding moiety between the spacer and the allosteric site residues was done using urea (in case of sorafenib) or amide (in case of sunitinib) moieties. In this regard, we designed our quinoxaline compounds with one or two amides pharmacophoric linking moiety containing HBA–HBD functional groups. The fourth strategy was to replace the terminal hydrophobic tail with other different hydrophobic moieties including aliphatic or substituted phenyl derivatives. The concept of using these hydrophobic moieties was to guarantee different lipophilic and electronic environments, which could result in additional hydrophobic interactions with the receptor.

2. Results and discussion

2.1 Chemistry

The classical method of quinoxaline preparation is to condensate phenylenediamine with a dicarbonyl compound.[38] This procedure requires high temperatures, a strong acid catalyst, and long reaction times. Other strategies described for the synthesis of quinoxaline derivatives involve 1,4-addition of 1,2-diamines to diazenylbutenes.[39] There are also several green synthetic methods *e.g.* one-pot synthesis,[40] microwave-assisted synthesis,[41] recyclable catalysts[42] and reactions in aqueous

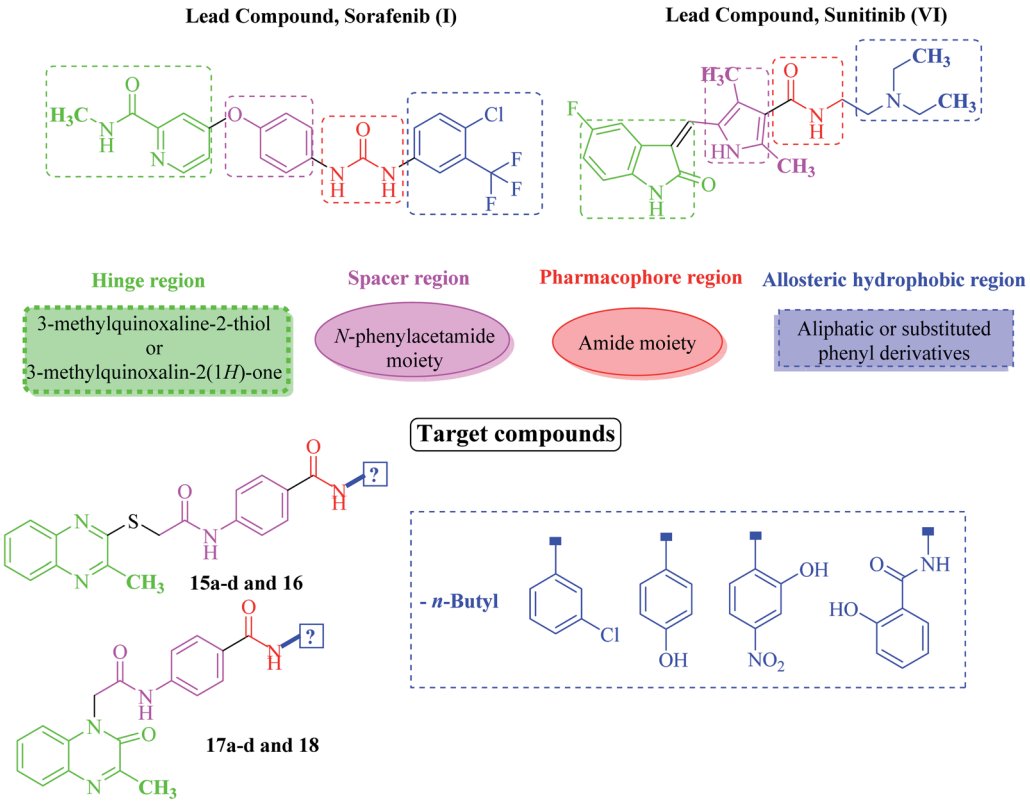

Fig. 2 Rational design of the new proposed VEGFR-2 inhibitors.

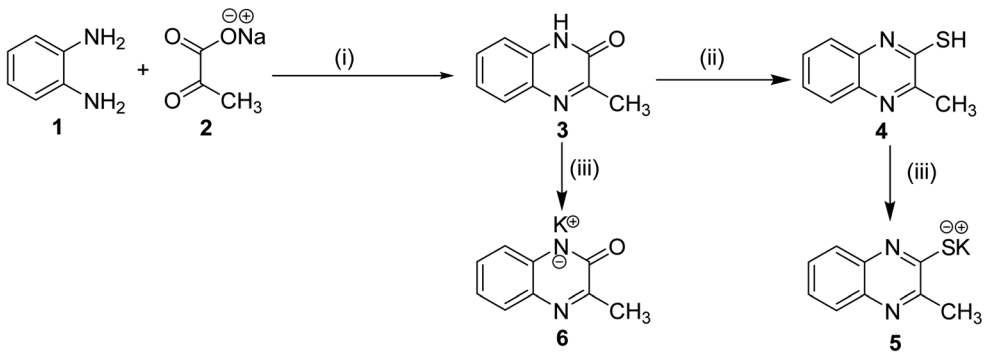

Scheme 1 General synthetic route of target salts **5** and **6**; reaction conditions: (i) glacial acetic acid/H_2O/reflux/2 h, (ii) thiourea/EtOH/reflux/6 h, (iii) Alc. KOH/reflux/30 min.

medium.[43] In this study and in the light of above findings, we used 3-methylquinoxalin-2(1*H*)-one as the scaffold to design new antitumor agents. For the synthesis of our target compounds, compounds **5**, **6**, **10a–d**, and **14** were initially synthesized according to the reported procedures[28,44] as outlined in Schemes 1 and 2.

The final compounds **15a–d**, **16**, **17a–d** and **18** were obtained in good yields following the reported procedures[45] described in Schemes 3 and 4.

2.2 Biological evaluation

2.2.1 ***In vitro*** **anti-proliferative activity.** MTT assay protocol was applied for all the tested compounds to evaluate their *in vitro* antiproliferative activities against MCF-7 and HepG-2.[46–48] Sorafenib was used as positive control. The results (IC_{50} values) were summarized in Table 1. Among the tested compounds, **15b** and **17b** were the most potent antiproliferative candidate. Comparing to sorafenib (IC_{50} = 3.51 and 2.17 μM against MCF-7 and HepG-2, respectively), compound **17b** (the most potent member) showed IC_{50} value of 2.3 μM and 2.8 μM against MCF-7 and HepG-2, respectively. In addition, compound **15b** exhibited IC_{50} value of 5.8 μM and 4.2 μM against MCF-7 and HepG-2, respectively.

2.2.2 ***In vitro*** **VEGFR-2 enzyme assay inhibition.** All final synthesized compounds were investigated for their VEGFR-2 inhibitory effect using sorafenib as a positive control. The

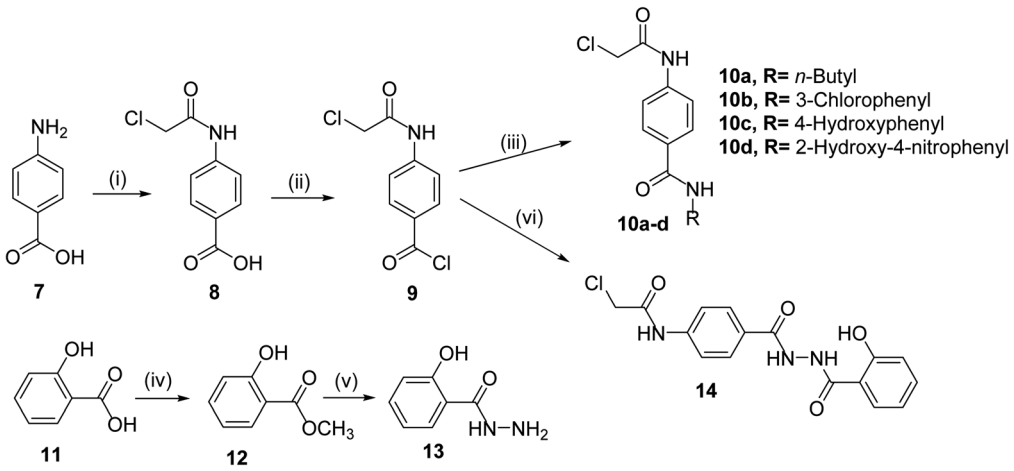

Scheme 2 : General synthetic route of target intermediates **10a–d** and **14**; reaction conditions: (i) $ClCH_2COCl/NaHCO_3$/DMF/r.t./1 h, (ii) $SOCl_2$/DMF/DCE/reflux/4 h, (iii) RNH_2/TEA/CH_3CN/r.t./8 h, (iv) CH_3OH/conc. H_2SO_4/reflux/8 h, (v) $NH_2NH_2 \cdot H_2O$/ethanol/reflux/8 h, (vi) **13**/TEA/CH_3CN/r.t./8 h.

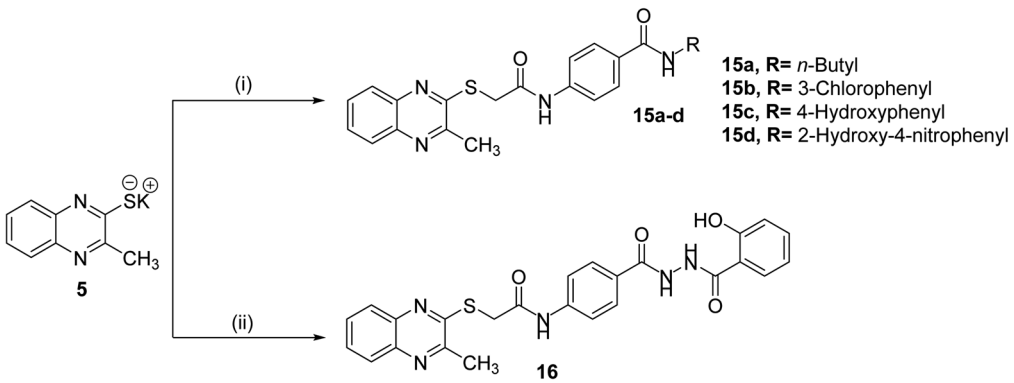

Scheme 3 General synthetic route of target final compounds **15a–d** and **16**; reaction conditions: (i) **10a–d**/cat. KI/DMF/WB/6 h, (ii) **14**/cat. KI/DMF/WB/6 h.

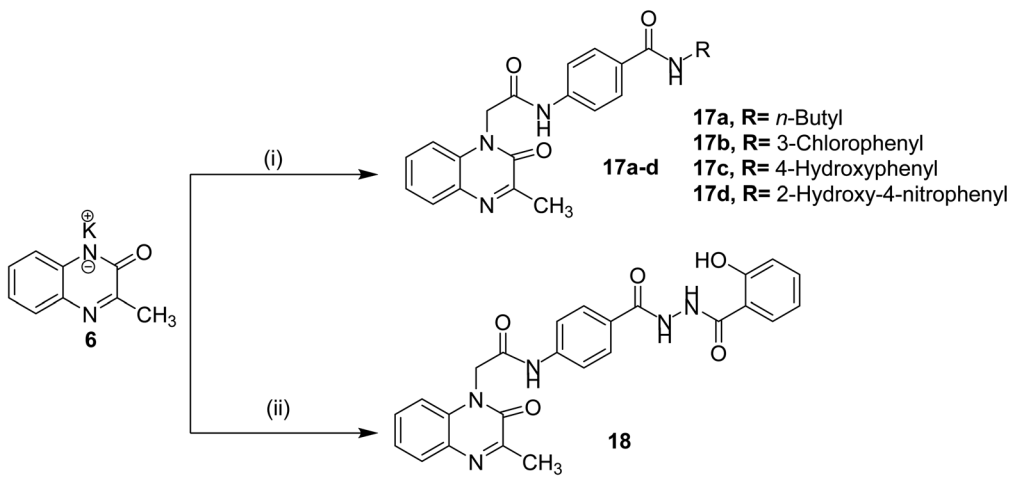

Scheme 4 General synthetic route of target final compounds **17a–d** and **18**; reaction conditions: (i) **10a–d**/cat. KI/DMF/WB/6 h, (ii) **14**/cat. KI/DMF/WB/6 h.

Table 1 *In vitro* anti-proliferative activities of the synthesized compounds against MCF-7 and HepG-2 cell lines, their VEGFR-2 inhibitory activities on cancer HepG-2, and cytotoxicity for compounds **17b** against normal hepatocytes

Comp.	MCF-7[a] (IC_{50}, μM)	HepG-2[a] (IC_{50}, μM)	VEGFR-2[a] (IC_{50}, nM)	Normal hepatocytes[a] (IC_{50}, μM)
15a	62.1 ± 3.2	41.2 ± 1.9	23.1 ± 0.8	NT[b]
15b	5.8 ± 0.6	4.2 ± 0.3	3.4 ± 0.2	NT[b]
15c	62.2 ± 2.9	50.4 ± 2.4	27.8 ± 1.2	NT[b]
15d	61.5 ± 2.3	42.8 ± 1.8	31.5 ± 1.3	NT[b]
16	35.8 ± 1.9	27.1 ± 1.2	18.5 ± 0.8	NT[b]
17a	29.3 ± 2.1	24.5 ± 1.0	11.2 ± 0.4	NT[b]
17b	2.8 ± 0.2	2.3 ± 0.2	2.7 ± 0.1	24.68 ± 1.3
17c	17.9 ± 0.6	14.3 ± 0.6	13.9 ± 0.5	NT[b]
17d	35.2 ± 1.6	22.4 ± 1.3	11.2 ± 0.3	NT[b]
18	22.3 ± 1.2	14.8 ± 0.5	11.2 ± 0.2	NT[b]
Sorafenib	3.51 ± 1.1	2.17 ± 0.1	3.12 ± 0.8	24.34 ± 1.6

[a] IC_{50} values are the mean ± S.D. (standard deviations) of three separate experiments. [b] NT: not tested.

Table 2 Values of different stages of cell cycle progression in HepG-2 after application of the most active compound **17b**

	Cell cycle analysis[a] (%)			
Sample	% Sub-G1	% G1	% S	% G2/M
HepG-2	1.56 ± 0.30	58.69 ± 2.04	28.94 ± 2.39	10.81 ± 0.22
17b/HepG-2	1.27 ± 0.17	40.03 ± 2.82**	28.31 ± 1.01	30.38 ± 2.93**

[a] Three independent experiments were applied for each value. **$p < 0.01$.

results (IC_{50} values) and reported in Table 1. Matching with the cytotoxicity results, compound **17b** was the most potent inhibitor with an IC_{50} value of 2.7 nM which was more than that of sorafenib (IC_{50} value 3.12 nM).

Based on the biological data, we can reach valuable SAR. It was found that the second series compounds **17a–d** and **18** (incorporating 3-methylquinoxalin-2(1*H*)-one) is more active than corresponding members **15a–d** and **16** (incorporating 3-methylquinoxaline-2-thiol). Such results indicate that 3-methylquinoxalin-2(1*H*)-one moiety is more advantageous than 3-methylquinoxaline-2-thiol moiety. The comparison between compounds containing aliphatic hydrophobic tail (**15a** and **17a** with IC_{50} values of 23.1 and 11.2 nM, respectively) and the corresponding members containing 3-chlorophenyl moiety (**15b** and **17b** with IC_{50} values of 3.4 and 2.7 nM, respectively) indicate that aromatic ring containing electron withdrawing group is more preferred biologically than aliphatic moiety. Comparing the IC_{50} values of compound **15b** and **17b** incorporating electron withdrawing group with their corresponding members **15c** and **17c** incorporating electron donating group, indicate that substitution with electron withdrawing group is more advantageous.

2.2.3 *In vitro* cytotoxicity against normal hepatic cells. One of the main problems of cancer chemotherapy is the unwanted damage to normal cells caused by the high toxicities of anticancer drugs. To assess the selectivity of the synthesized compounds against cancer cells over normal ones, the cytotoxicity of compound **17b** was evaluated *in vitro* against primary rat hepatocytes using sorafenib as reference.[49] The results revealed that **17b** showed cytotoxic activity against cancer HepG-2 cell line (10-fold) more than cytotoxic activity against normal hepatic cells in comparison to sorafenib (11-fold), Table 1. Such results indicate that compound **17b** has a significant effect in rapidly proliferating cells but not in normal cells.

2.2.4 Effect of 17b on cell cycle progression. The effect of compound **17b** on the cell cycle distribution was evaluated against HepG-2 cells.[50] In this method, HepG-2 cells were treated with **17b** (2.3 μM, IC_{50} value) and the technique was carried out according to the reported procedure. The results (Table 2 and Fig. 3) revealed that compound **17b** arrested cell growth in G2-M phase, accretion of cells at that phase became 30.38% after being 10.81 in control cells. The apoptosis data for compound **17b** is described in ESI.†

2.2.5 Effects of 17b on the apoptotic markers, caspases, BAX, and Bcl-2. In the current study, western plot technique was utilized for compound **17b** (2.3 μM) to investigate its effect on the expression levels of caspases, BAX, and Bcl-2. Our results showed that compound **17b** clearly increased the level of caspase-3 by 1.8 fold and caspase-9 by 1.74 fold compared to the control cells (Fig. 4). Also, the results showed that **17b** boosted the level of BAX by approximately 4-fold. Moreover, compound **17b** markedly downregulated the levels of Bcl-2 by around 3-fold. Finally, compound **17b** interestingly boosted the Bax/Bcl-2 ratio by more than 10-fold (Table 3).

2.3 *In silico* studies

2.3.1 Molecular docking against VEGFR-2. Molecular Operating Environment MOE, package version 2014.09 software

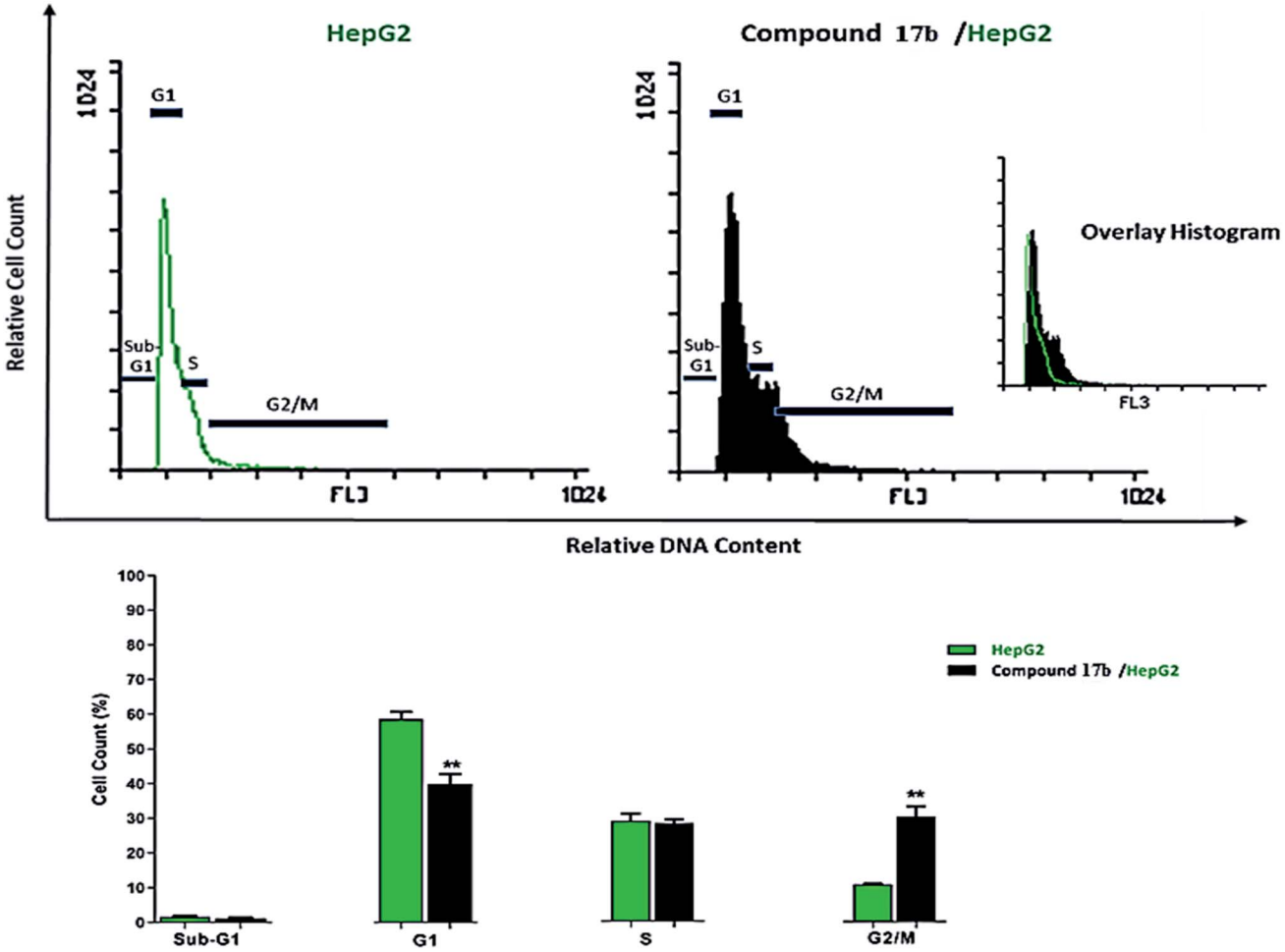

Fig. 3 Cycle phases after the treatment with compound **17b**, $^{**}p < 0.01$.

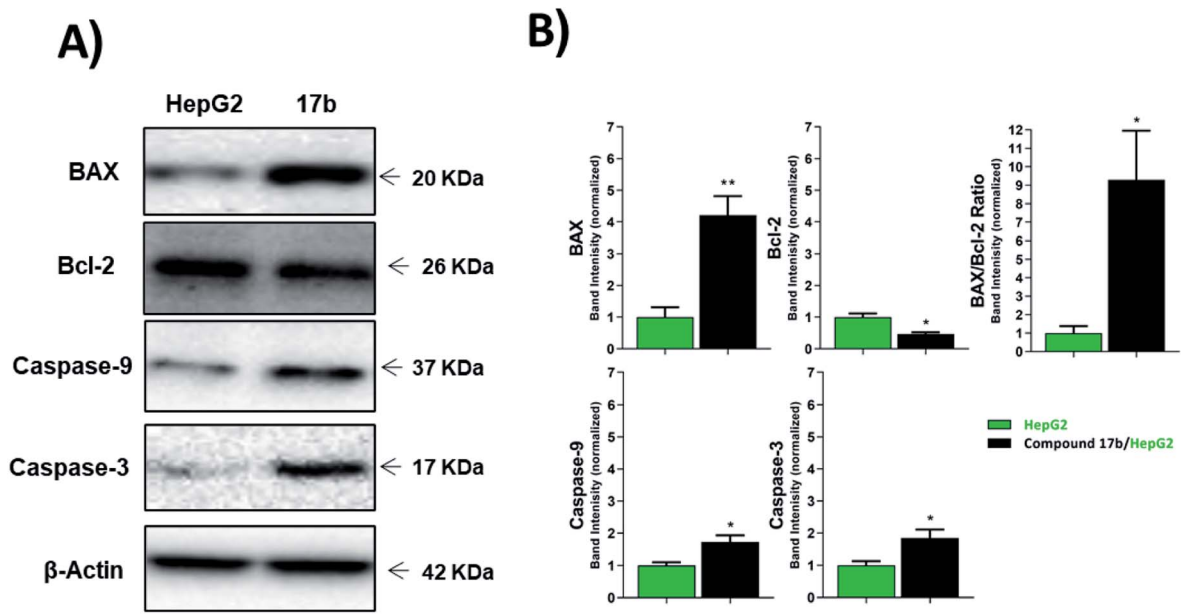

Fig. 4 The immunoblotting of the apoptotic markers (normalized to β-actin). $^{*}p < 0.05$, $^{**}p < 0.01$, $^{***}p < 0.001$.

Table 3 Effect of compound **17b** on levels of BAX, Bcl-2, active caspases-9, and active caspases-3 protein expression in HepG-2 cells treated for 24 h.

	Protein expression (normalized to β-actin)[a]				
Sample	BAX	Bcl-2	BAX/Bcl-2 ratio	Caspases-9	Caspases-3
HepG-2	1.00 ± 0.31	1.00 ± 0.12	1.00 ± 0.38	1.00 ± 0.10	1.00 ± 0.13
17b/HepG-2	4.21 ± 0.60**	0.32 ± 0.04*	9.30 ± 2.66*	1.74 ± 0.20*	1.85 ± 0.26*

[a] Values are given as mean ± SEM of three independent experiments. *$p < 0.05$ and **$p < 0.01$ indicate statistically significant differences from the corresponding control (HepG-2) group in unpaired t-tests.

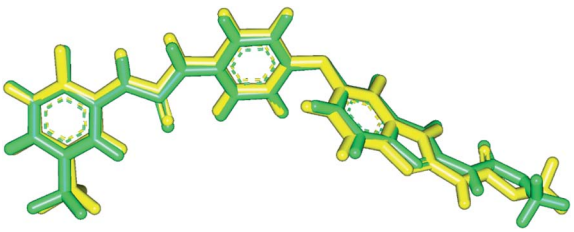

Fig. 5 Validation of the docking process.

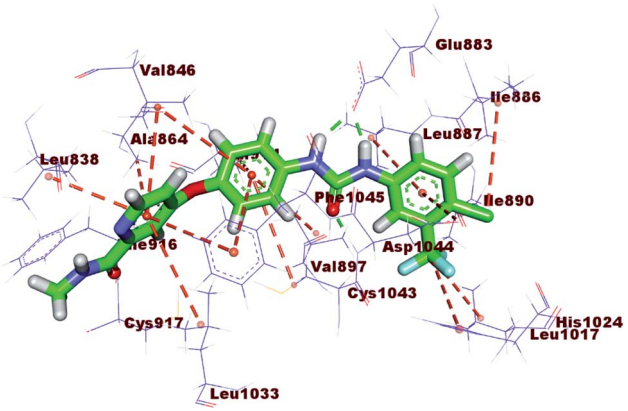

Fig. 6 Interaction of sorafenib with the essential amino acids inside VEGFR-2 active site.

was used for the docking simulations against VEGFR-2 kinase to rationalize the obtained biological results. At the beginning, validation of the docking process was verified and the RMSD value was 0.48 which indicated the validity of the docking process (Fig. 5). The binding pattern of sorafenib to VEGFR-2 active site has been explained in Fig. 6. And the results were matched with the reported data.[18,51] The energy scores of the tested candidates and sorafenib were summarized in Table 4.

The mode of interaction of compound **15b** against VEGFR-2 active site was the same of sorafenib ($\Delta G = -23.27$ kcal mol^{-1}). The amide group was involved in two hydrogen bonds, where the amidic NH formed a hydrogen bond with the carboxylate moiety of Glu883 (2.66 Å) and the carbonyl group formed another hydrogen bond with the NH of Asp1044 (3.0 Å). Additionally, the quinoxaline moiety occupied the hinge region forming two hydrophobic interactions with Leu383 and Phe916. The central phenyl ring formed three hydrophobic interactions with Val897, Val914, and Cys1043. The terminal 3-chlorophenyl

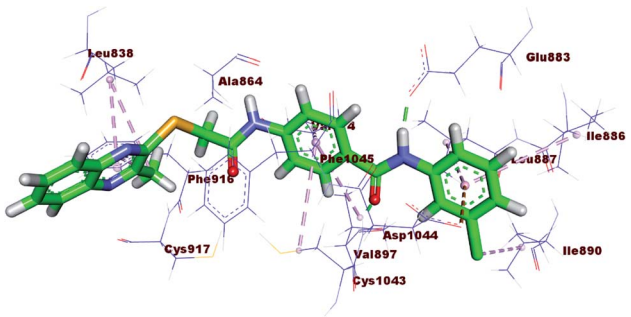

Fig. 7 3D representation of **15b** with VEGFR-2.

Table 4 The calculated ΔG (binding free energies) of the synthesized compounds, sorafenib, and co-crystallized ligand against VEGFR-2 (ΔG in kcal mol^{-1})

Comp.	ΔG [kcal mol^{-1}]	Comp.	ΔG [kcal mol^{-1}]
15a	−24.63	**17b**	−23.97
15b	−23.27	**17c**	−23.62
15c	−23.03	**17d**	−23.67
15d	−23.47	**18**	−24.14
16	−22.33	Sorafenib	−22.15
17a	−24.89		

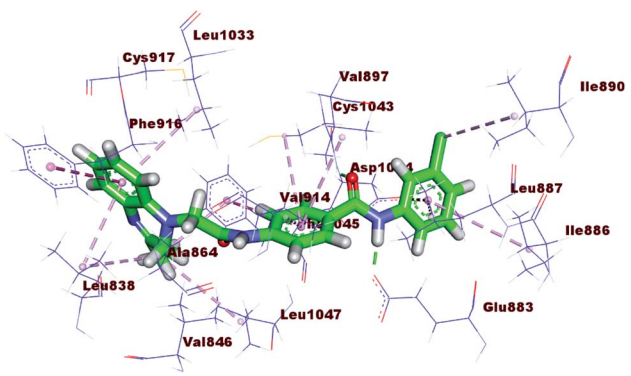

Fig. 8 3D representation of **17b** with VEGFR-2.

Table 5 The binding free energies of **17b** and PKT against cytochrome P450 (PDB ID: 4D7D)

Comp.	Binding free energy (kcal mol^{-1})	No. of hydrogen bonds	No. of electrostatic interaction	No. of hydrophobic interaction
17b	−16.05	0	0	5
PKT	−25.73	1	1	7

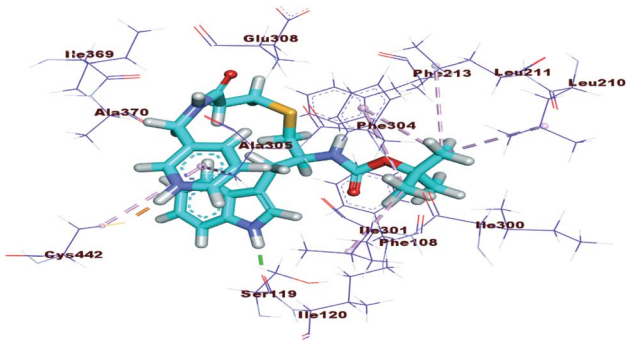

Fig. 9 3D Structure of PKT docked into active pocket of cytochrome P450.

moiety was involved in three hydrophobic moieties with Ile890, Lue887, and Ile886. In addition, it formed one electrostatic interaction with Asp1044 (Fig. 7).

The docking results of compound **17b** (ΔG = −23.97 kcal mol^{-1}) are nearly similar to that of sorafenib. In the DFG region, –NH of the amide moiety in the pharmacophore region formed a hydrogen bond with the carboxylate moiety of Glu883 (1.72 Å). Also, carbonyl group of the amide moiety formed another hydrogen bond with the NH of Asp1044 (2.99 Å). In addition, the terminal hydrophobic (3-chlorophenyl moiety) formed three hydrophobic interactions with Leu887, Ile886, and Ile890. Also, it formed electrostatic interaction with Asp1044. Moreover, the quinoxaline moiety occupied the hinge region forming five hydrophobic interactions with Leu1033, Phe916, Leu838, Phe1045, and Leu1047. The central phenyl group formed four hydrophobic bonds with Val914, Val897, Cys1043, and Phe1045. Such binding pattern may explain the promising biological activity of this member comparing the other candidates (Fig. 8).

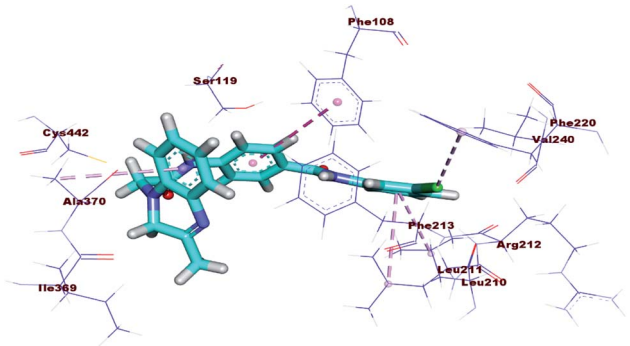

Fig. 10 3D Structure of **17b** docked into active pocket of cytochrome P450.

The binding modes of compounds **16** and **18** are depicted in ESI.† All figures in our docking study were visualized using Discovery Studio Visualizer.

2.3.2 Molecular docking for compound 17b against cytochrome P450. In this work, further molecular docking investigational study was performed for the most active compound against cytochrome P450 3A4 (CYP3A4). This study was carried out to gain further insight into the binding modes of the most active compound into the binding site of CYP3A4 (PDB ID: 4D7D). The co-crystallized ligand (PKT) was used as a reference molecule. The binding free energies (ΔG) were reported in Table 5.

The proposed binding mode of PKT showed binding energy of −25.73 kcal mol^{-1}. It formed one hydrogen bond with Ser119 and one electrostatic bond with Cys442. In addition, it formed seven hydrophobic interactions with Leu210, Leu211, Ile301, Ala305, and Phe304 (Fig. 9).

The proposed binding mode of **17b** was illustrated in Fig. 10 with binding energy −16.05 kcal mol^{-1}, far less than that of the co-crystallized ligand. In addition, the binding mode of this compound was different from that of the co-crystallized ligand. These results revealed that **17b** cannot be CYP3A4 inhibitors and consequently indicates its less liver toxicity.

2.3.3 *In silico* ADMET studies for compounds 15b and 17b. Blood–brain barrier (BBB) penetration, intestinal absorption, aqueous solubility, CYP2D6 binding, and plasma protein binding properties of compounds **15b** and **17b** were calculated using Discovery studio 4.0. The BBB penetration levels of the tested compounds were in the low and very low range. Depending on these results, it may be concluded that there are no CNS side effects associated with these compounds. In addition, compounds **15b** and **17b** showed good levels of intestinal absorption and aqueous solubility. For cytochrome P450 2D6 (CYP2D6) inhibition, both of them were predicted as non-inhibitors. Finally, **15b** and **17b** were expected to bind plasma protein more than 90% (Table 6). *In silico* ADMET studies for the rest of the compounds are explained in ESI.†

2.3.4 *In silico* toxicity studies for compounds 15b and 17b. Toxicity profile of compounds **15b** and **17b** were predicted according to the built-in models of Discovery studio 4.0 software using seven toxicity parameters.[52,53]

At first, the carcinogenic potency TD_{50} values (from 9.366 to 142.906 mg per kg body weight per day) of the tested compounds were higher than that of the reference molecule; sorafenib (TD_{50} = 19.236 mg per kg body weight per day). In addition, the maximum tolerated dose values (from 0.096 to 0.333 g per kg body weight) of both compounds were higher than sorafenib (0.089 g per kg body weight). Furthermore, the tested compounds showed oral LD_{50} values ranging from 4.703

Table 6 ADMET parameters for compounds **15b** and **17b**

Comp.	BBB level[a]	Solubility level[b]	Absorption level[c]	CYP2D6 prediction[d]	PPB prediction[e]
15b	++++	++	0	F	More than 90%
17b	+++	++	0	F	More than 90%
Sorafenib	++++	+	0	F	More than 90%

[a] BBB level, 0 = very high, + = high, ++ = medium, +++ = low, ++++ = very low. [b] Solubility level, + = very low, ++ = low, +++ = good, ++++ = optimal. [c] Absorption level, 0 = good, + = moderate, ++ = poor, ++ = very poor. [d] CYP2D6, cytochrome P2D6, T = inhibitor, F = non inhibitor. [e] PBB, plasma protein binding (less than 90% or more than 90%).

Table 7 Physico-chemical properties of **15b**, **17b** and sorafenib

Comp.	*A* log *P*[a]	log *D*[b]	MPSA[c]	MSA[d]	MV[e]	HBA[f]	HBD[g]	M. WT[h]
15b	4.74	4.74	109.28	444.39	339.56	6	2	462.951
17b	3.12	3.12	90.87	430.37	328.25	7	2	446.886
Sorafenib	4.17	4.17	92.35	434.9	323.1	7	3	464.825

[a] Log of the octanol–water partition coefficient. [b] The octanol–water partition coefficient calculated considering the ionization states of the molecule. [c] Molecular surface area: calculates the total surface area for each molecule using a 2D approximation. [d] Molecular polar surface area: calculates the polar surface area for each molecule using a 2D approximation. [e] Molecular volume: calculates the 3D volume for each molecule using the current 3D coordinates. [f] Hydrogen bond acceptor atoms. [g] Hydrogen bond donor atoms. [h] Molecular weight.

Table 8 Thermodynamic parameters of compounds **15b**, **17b** and sorafenib

Name	Total energy (kcal mol^{-1})	Binding energy (kcal mol^{-1})	HOMO energy (kcal mol^{-1})	LUMO energy (kcal mol^{-1})	Gap energy	μ
15b	−2139.791	−10.576	−0.200	−0.107	0.093	2.365
17b	−1817.724	−10.717	−0.201	−0.103	0.098	3.061
Sorafenib	−2000.377	−9.866	−0.200	−0.091	0.109	3.088

to 12.496 mg per kg body weight per day which were higher than that of sorafenib (0.823 mg per kg body weight per day). For rat chronic lowest observed adverse effect level (LOAEL), the tested molecules showed higher values (from 0.072 to 0.583 g per kg body weight) than sorafenib (0.005 g per kg body weight). Moreover, the tested compounds were predicted to be mild irritant against eyes and non-irritant against skin. For aerobic biodegradability model, all compounds were anticipated to be non-degradable. *In silico* toxicity studies for the synthesized compounds are explained in ESI.†

2.3.5 Physico-chemical properties of compounds 15b and 17b. The *A* log *P* values express the degree of lipophilicity of the chemical compound, where the log *D* values express the degree of lipophilicity of the chemical compound taking into account the ionization states of the molecule.[54] An increase in these values indicates an increase in the lipophilic character of the tested compound. It is worthwhile to note that the *A* log *P* and log *D* values for most compounds in acceptable range for oral and intestinal absorption (1.44–4.74).[55]

In addition, the molecular polar surface area (MPSA) is another key property linked to drug bioavailability; the passively absorbed molecules with MPSA >140 have low oral bioavailability.[56] Compounds **15b** and **17b** showed acceptable values of MPSA less than 140. Moreover, molecular volume (MV) descriptor determines transport characteristics of molecules, such as intestinal absorption.[57] The drug diffusivity is inversely proportional to the molecular volume. Molecules with lower MV have higher diffusivity.[58] It was observed that both compounds exhibited low molecular volume values (from 315.21 to 353.63) when compared with sorafenib (MV = 323.1). Finally, Lipinski rule of five was applied for compounds **15b** and **17b**. It was found that both of them have molecular weight less than 500, hydrogen bond acceptor groups less than 10, and hydrogen bond donor group less than 5. This indicates that these compounds are likely to be orally bioavailable (Table 7). Physico-chemical properties for the rest of the compounds are explained in ESI.†

2.3.6 DFT studies for compound 15b and 17b. Discovery studio software was used to carry out density functional theory (DFT) calculations. Different molecular and atomic properties were calculated including (i) total energy of the molecules, (ii) binding energy which describes the interaction energy between all the atoms in the molecule, (iii) the energy of the highest occupied molecular orbital (HOMO), (iv) the energy of the lowest unoccupied molecular orbital (LUMO), gap energy which describes the energy difference between LUMO and HOMO, (v) the magnitude of the dipole moment (μ).

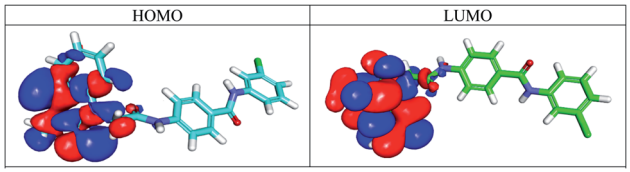

Fig. 11 Spatial distribution of molecular orbitals for **17b**.

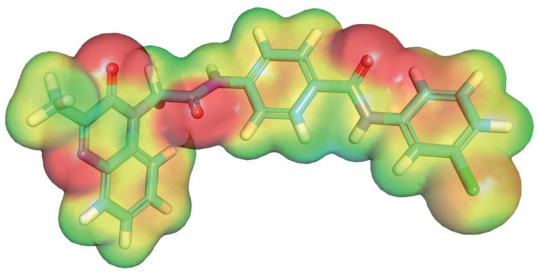

Fig. 12 Molecular electrostatic potential map of compound **17b**.

The results (Table 8) revealed that the total energies of compounds **15b**, **17b** and sorafenib have negative values which are favorable for spontaneous binding and interaction. In addition, both **15b** and **17b** have dipole moment values very close to that of sorafenib. The improved dipole moment can enhance hydrogen bond and non-bonded interactions in drug receptor complexes which keep an important role to increase binding affinity. Elevated dipole moment indicated the increased binding affinity with target enzyme during VEGFR-2 inhibitory activities. Thermodynamic parameters for the rest of the compounds are explained in ESI.†

*2.3.6.1 Molecular orbital analysis for compound **17b**.* According to the frontier molecular orbital theory, the energies of HOMO and LUMO play an important role in chemical reactivity.[59] It was evident that compound **17b** have gap energy values very close to that of sorafenib. Fig. 11 showed the spatial distribution of molecular orbitals for compound **17b**. Molecular orbital analysis for sorafenib and compound **15b** are depicted in ESI.†

*2.3.6.2 Electrostatic potential map for compound **17b**.* Electrostatic interactions are one of the forces guiding the binding of molecules to proteins. The assessment of this interaction through computational approaches makes it possible to evaluate the energy of protein–drug complexes.[60] Next to steric complementarity, electrostatics are one of the main driving forces involved in molecular recognition.[61] Electrostatics are known to play a key role in protein–DNA,[62] protein–protein[63] and protein–substrate[61] recognitions.

There are many colored patches in MEP surface according to availability of electron cloud. Atoms with high electronegativity and negative charges display red color and can form hydrogen bonding acceptor. While atoms with poor electron and positive charge display blue color and can form hydrogen bonding donor. The atoms with zero charge values display green to yellow color and can form π- and other types of staking interactions. This molecular detail helps to predict how much they are potential to take part in chemical reactions and to realize their mechanism of interactions.[64]

The most active compound **17b** showed MEP map like that of sorafenib to some extent. The quinoxaline moiety showed a red patch at the nitrogen atoms and carbonyl group which can form hydrogen bond with polar amino acids at the hinge region. The two amide groups in each molecule showed red and blue patches which indicate the possibility of hydrogen bond formation. The aromatic moieties in each molecule showed high electron cloud (green to yellow patches) which can favor the π-staking interaction with aromatic amino acid residues (Fig. 12). Molecular electrostatic potential map for sorafenib and **15b** are depicted in ESI.†

3. Conclusion

In the presented work ten quinoxaline derivatives (**15a–d**, **16**, **17a–d**, and **18**) were designed and synthesized. Compound **17b** was the most promising candidate against MCF-7, HepG-2, and VEGFR-2 with IC_{50} values of 2.8 μM, 2.3 μM, and 2.7 nM respectively, more than that of sorafenib 3.51 μM, 2.17 μM, and 3.12 nM respectively. Also, compound **17b** arrested the cell cycle in the G2/M phase and induced apoptosis in HepG-2 cells. Moreover, the mentioned compound upregulated the level caspase-3, caspase-9 and boosted the Bax/Bcl-2 ratio by more than 10-fold, as compared to the control. Docking studies revealed that most compounds have similar binding pattern with VEGFR-2. *In silico* ADMET, toxicity, and physico-chemical properties divulged that target compounds exhibited acceptable pharmacokinetic profile, and physicochemical properties. Further docking studies for compound **17b** against cytochrome P450 showed the non-inhibitory effect of this compound. DFT calculations including total energy, binding energy, HOMO, LUMO, gap energy, dipole moment, and electrostatic potential were performed. The development of other VEGFR-2 inhibitors involving quinoxaline derivatives is ongoing and will be reported in due course.

4. Experimental

4.1 Chemistry

All the reagents, chemicals, apparatus were described in ESI.† Compounds **3**, **4**, **5**, **6**, **8**, **9**, **10a–d**, **12**, **13**, and **14** were obtained according to the reported procedures.[29,65–68]

4.1.1 General procedure for preparation of the target compounds 15a–d and 16. A mixture of potassium 3-methylquinoxaline-2-thiolate **5** (0.214 g, 0.001 mol) and the appropriate 4-(2-chloroacetamido)-*N*-(substituted)benzamide **10a–d** (0.001 mol) or 2-chloro-*N*-(4-(2-(2-hydroxybenzoyl) hydrazine-1-carbonyl)phenyl)acetamide **14** (0.001 mol), anhydrous K_2CO_3 (0.001 mol) and KI (0.001 mol) in DMF (10 ml) was heated on a water bath for 8 h. The reaction mixture was then poured on crushed ice. The precipitates were filtered, dried, and crystalized from methanol to give the corresponding target compounds **15a–d** and **16**.

4.1.1.1 N-Butyl-4-(2-((3-methylquinoxalin-2-yl)thio) acetamido)benzamide ***15a***. Yellow crystal (yield, 65%); mp = 190–192 °C; FT-IR (ν max, cm^{-1}): 3370, 3273, 3100, 2956, 2931, 1674, 1621, 1536; ^{1}H NMR (700 MHz, DMSO-d_6) δ 10.66 (s, 1H), 8.32 (t, J = 5.6 Hz, 1H), 7.97–7.95 (m, 1H), 7.82 (d, J = 6.0 Hz, 1H), 7.81 (d, J = 6.8 Hz, 2H), 7.73–7.69 (m, 2H), 7.69–7.67 (m, 2H), 4.30 (s, 2H), 3.24 (td, J = 7.1, 5.6 Hz, 2H), 2.67 (s, 3H), 1.51–1.48 (m, 2H), 1.34–1.31 (m, 2H), 0.90 (t, J = 7.4 Hz, 3H); ^{13}C NMR (176 MHz, DMSO-d_6) δ 166.93, 165.98, 155.45, 151.97, 141.89, 140.81, 139.34, 130.03, 129.90, 128.91, 128.67, 128.53, 127.37, 118.71, 39.27, 35.38, 31.78, 22.18, 20.14, 14.21; MS (m/z): exact mass calcd for $C_{22}H_{24}N_4O_2S$ $[M]^+$: 408.2. Found: 408.2. Anal. calcd for $C_{22}H_{24}N_4O_2S$: C, 64.68; H, 5.92; N, 13.71. Found: C, 63.86; H, 6.00; N, 13.34.

4.1.1.2 N-(3-Chlorophenyl)-4-(2-((3-methylquinoxalin-2-yl) thio)acetamido)benzamide, ***15b***. Reddish white crystal (yield, 75%); mp = 223–225 °C; FT-IR (ν max, cm^{-1}): 3400, 3270, 2900, 1668, 1644, 1592; ^{1}H NMR (700 MHz, DMSO-d_6) δ 10.77 (s, 1H), 10.29 (s, 1H), 7.98–7.95 (m, 4H), 7.83 (dd, J = 8.2, 1.6 Hz, 1H), 7.79 (d, J = 8.6 Hz, 2H), 7.72–7.68 (m, 3H), 7.38 (t, J = 8.1 Hz, 1H), 7.15 (dd, J = 8.1, 2.1 Hz, 1H), 4.33 (s, 2H), 2.67 (s, 3H); ^{13}C NMR (176 MHz, DMSO-d_6) δ 167.12, 165.58, 155.43, 151.96, 142.71, 141.25, 140.81, 139.36, 133.39, 130.75, 130.02, 129.45, 129.30, 128.90, 128.68, 127.37, 123.63, 120.09, 119.02, 118.82, 35.43, 22.18; MS (m/z): exact mass calcd for $C_{24}H_{19}ClN_4O_2S$ $[M]^+$: 462.1. Found: 463.0. Anal. calcd for $C_{24}H_{19}ClN_4O_2S$: C, 62.27; H, 4.14; N, 12.10. Found: C, 61.91; H, 3.92; N, 11.57.

4.1.1.3 N-(4-Hydroxyphenyl)-4-(2-((3-methylquinoxalin-2-yl) thio)acetamido)benzamide ***15c***. Deep brown crystal (yield, 70%); mp = 250–252 °C; FT-IR (ν max, cm^{-1}): 3450, 3318, 2910, 1669, 1601, 1511; ^{1}H NMR (700 MHz, DMSO-d_6) δ 10.91 (s, 1H), 10.76 (s, 1H), 10.24 (s, 1H), 8.13–8.11 (m, 2H), 7.97 (d, J = 4.3 Hz, 2H), 7.84 (d, J = 8.5 Hz, 2H), 7.80–7.77 (m, 2H), 7.72–7.69 (m, 2H), 7.26–7.24 (m, 2H), 4.34 (s, 2H), 2.68 (s, 3H); ^{13}C NMR (176 MHz, DMSO-d_6) δ 167.40, 167.08, 155.46, 151.98, 140.81, 139.37, 131.61, 130.06, 129.22, 128.93, 128.69, 127.38, 122.46, 121.72, 119.08, 118.80, 115.41, 35.50, 22.19; MS (m/z): exact mass calcd for $C_{24}H_{20}N_4O_3S$ $[M]^+$: 444.1. Found: 445.1. Anal. calcd for $C_{24}H_{20}N_4O_3S$: C, 64.85; H, 4.54; N, 12.60. Found: C, 64.8; H, 4.86; N, 12.04.

4.1.1.4 N-(2-Hydroxy-4-nitrophenyl)-4-(2-((3-methylquinoxalin-2-yl)thio)acetamido)benzamide ***15d***. Yellow crystal (yield, 80%); mp = 195–197 °C; FT-IR (ν max, cm^{-1}): 3450, 3269, 2910, 1671, 1594, 1508; ^{1}H NMR (700 MHz, DMSO-d_6) δ 11.15 (s, 1H), 10.81 (s, 1H), 9.49 (s, 1H), 8.25 (dd, J = 9.4, 3.9 Hz, 1H), 8.08–8.02 (m, 2H), 7.98 (d, J = 7.7 Hz, 2H), 7.96 (d, J = 4.5 Hz, 2H), 7.83 (d, J = 8.5 Hz, 2H), 7.73 (d, J = 8.4 Hz, 2H), 4.33 (s, 2H), 2.68 (s, 3H); ^{13}C NMR (176 MHz, DMSO-d_6) δ 167.18, 165.11, 162.78, 155.44, 151.97, 148.61, 143.65, 143.06, 140.81, 139.36, 133.68, 130.05, 129.27, 128.92, 128.69, 127.38, 121.80, 119.00, 109.89, 36.26, 35.46, 31.24, 22.19; MS (m/z): exact mass calcd for $C_{24}H_{19}N_5O_5S$ $[M]^+$: 489.1. Found: 490.0. Anal. calcd for $C_{24}H_{19}N_5O_5S$: C, 58.89; H, 3.91; N, 14.31. Found: C, 58.48; H, 3.58; N, 14.94.

4.1.1.5 N-(4-(2-(2-Hydroxybenzoyl)hydrazine-1-carbonyl) phenyl)-2-((3-methylquinoxalin-2-yl)thio)acetamide ***16***. Deep brown crystal (yield, 55%); mp = 208–210 °C; FT-IR (ν max, cm^{-1}): 3450, 3261, 2910, 1647, 1603, 1524; ^{1}H NMR (700 MHz, DMSO-d_6) δ 11.97 (s, 1H), 10.76 (s, 1H), 10.67–10.66 (m, 1H), 10.58 (s, 1H), 7.95 (d, J = 1.7 Hz, 2H), 7.77 (d, J = 8.5 Hz, 2H), 7.47 (d, J = 7.0 Hz, 2H), 7.00–6.98 (m, 4H), 6.96 (d, J = 7.1 Hz, 2H), 4.33 (s, 2H), 2.68 (s, 3H); ^{13}C NMR (176 MHz, DMSO-d_6) δ 168.28, 167.12, 165.49, 162.78, 159.80, 155.44, 151.97, 142.78, 140.82, 139.36, 134.66, 130.05, 129.06, 128.73, 119.53, 118.91, 117.88, 115.00, 36.26, 35.45, 31.24, 22.19; MS (m/z): exact mass calcd for $C_{25}H_{21}N_5O_4S$ $[M]^+$: 487.1. Found: 488.1. Anal. calcd for $C_{25}H_{21}N_5O_4S$: C, 61.59; H, 4.34; N, 14.37. Found: C, 62.2; H, 3.9; N, 13.27.

4.1.2 General procedure for preparation of the target compounds 17a–d and 18. A mixture of potassium 3-methylquinoxaline-2-thiolate **6** (0.198 g, 0.001 mol) and the appropriate 4-(2-chloroacetamido)-*N*-(substituted)benzamide **10a–d** (0.001 mol) or 2-chloro-*N*-(4-(2-(2-hydroxybenzoyl) hydrazine-1-carbonyl)phenyl)acetamide **14** (0.001 mol), anhydrous K_2CO_3 (0.001 mol) and KI (0.001 mol) in DMF (10 ml) was heated on a water bath for 8 h. Next, the reaction mixture was poured on crushed ice. The precipitates were filtered, dried, and crystalized from methanol to give the final compounds **17a–d** and **18**.

4.1.2.1 N-Butyl-4-(2-(3-methyl-2-oxoquinoxalin-1(2H)-yl)acetamido)benzamide ***17a***. White crystal (yield, 60%); mp = 279–281 °C; FT-IR (ν max, cm^{-1}): 3429, 3318, 2910, 1647, 1601, 1530; ^{1}H NMR (700 MHz, DMSO-d_6) δ 10.68 (s, 1H), 8.33 (t, J = 5.6 Hz, 1H), 7.83–7.81 (m, 2H), 7.81–7.78 (m, 1H), 7.65–7.63 (m, 2H), 7.57 (ddd, J = 8.6, 7.1, 1.5 Hz, 1H), 7.52 (dd, J = 8.5, 1.2 Hz, 1H), 7.38 (ddd, J = 8.2, 7.1, 1.2 Hz, 1H), 5.16 (s, 2H), 3.24 (td, J = 7.1, 5.6 Hz, 2H), 2.49 (s, 3H), 1.50 (ddd, J = 8.6, 6.3, 1.9 Hz, 2H), 1.34–1.31 (m, 2H), 0.90 (t, J = 7.4 Hz, 3H); ^{13}C NMR (176 MHz, DMSO-d_6) δ 165.91, 165.67, 157.97, 154.85, 141.43, 133.46, 132.46, 130.19, 130.05, 129.27, 128.56, 123.93, 118.76, 115.19, 45.75, 39.28, 31.76, 21.59, 20.14, 14.21; MS (m/z): exact mass calcd for $C_{22}H_{24}N_4O_3$ $[M]^+$: 392.2. Found: 392.2. Anal. calcd for $C_{22}H_{24}N_4O_3$: C, 67.33; H, 6.16; N, 14.28. Found: C, 67.72; H, 5.87; N, 13.38.

4.1.2.2 N-(3-Chlorophenyl)-4-(2-(3-methyl-2-oxoquinoxalin-1(2H)-yl)acetamido)benzamide ***17b***. Yellow crystal (yield, 65%); mp >300 °C; FT-IR (ν max, cm^{-1}): 3429, 3318, 2910, 1640, 1603, 1524; ^{1}H NMR (700 MHz, DMSO-d_6) δ 10.80 (s, 1H), 10.31 (s, 1H), 7.98–7.96 (m, 3H), 7.81 (dd, J = 8.0, 1.5 Hz, 1H), 7.74–7.73 (m, 2H), 7.71–7.70 (m, 1H), 7.59–7.57 (m, 1H), 7.54 (dd, J = 8.5, 1.3 Hz, 1H), 7.40–7.37 (m, 2H), 7.16 (ddd, J = 8.0, 2.1, 0.9 Hz, 1H), 5.19 (s, 2H), 2.49 (s, 3H); ^{13}C NMR (176 MHz, DMSO-d_6) δ 165.85, 165.48, 157.97, 154.85, 142.25, 141.22, 133.47, 133.38, 132.47, 130.78, 130.20, 129.57, 129.33, 129.29, 123.95, 123.66, 120.11, 119.05, 118.87, 115.21, 45.80, 21.59; MS (m/z): exact mass calcd for $C_{24}H_{19}ClN_4O_3$ $[M]^+$: 446.1. Found: 447.1. Anal. calcd for $C_{24}H_{19}ClN_4O_3$: C, 64.50; H, 4.29; N, 12.54. Found: C, 64.98; H, 4.05; N, 12.09.

4.1.2.3 N-(4-Hydroxyphenyl)-4-(2-(3-methyl-2-oxoquinoxalin-1(2H)-yl)acetamido)benzamide ***17c***. Yellowish white crystal (yield, 70%); mp >300 °C; FT-IR (ν max, cm^{-1}): 3303, 3261, 2958, 1644, 1601, 1513; ^{1}H NMR (700 MHz, DMSO-d_6) δ 10.75 (s, 1H), 9.93 (s, 1H), 9.25 (s, 1H), 7.94 (d, J = 8.6 Hz, 2H), 7.70 (d, J = 8.5 Hz, 2H),

7.58–7.56 (m, 1H), 7.54–7.53 (m, 2H), 7.52 (d, J = 2.2 Hz, 2H), 7.38 (d, J = 7.4 Hz, 1H), 6.74–6.73 (m, 2H), 5.18 (s, 2H), 2.49 (s, 3H); ^{13}C NMR (176 MHz, DMSO-d_6) δ 165.75, 164.67, 157.97, 154.85, 154.08, 133.46, 132.47, 131.21, 130.28, 130.20, 129.28, 129.01, 123.94, 122.72, 118.81, 115.41, 115.20, 45.78, 21.59; MS (m/z): exact mass calcd for $C_{24}H_{20}N_4O_4$ $[M]^+$: 428.1. Found: 429.1. Anal. calcd for $C_{24}H_{20}N_4O_4$: C, 67.28; H, 4.71; N, 13.08. Found: C, 67.08; H, 4.48; N, 12.87.

4.1.2.4 N-(2-Hydroxy-4-nitrophenyl)-4-(2-(3-methyl-2-oxoquinoxalin-1(2H)-yl)acetamido)benzamide ***17d.*** Deep yellow crystal (yield, 70%); mp >300 °C; FT-IR (ν max, cm^{-1}): 3353, 3261, 2958, 1711, 1667, 1597; ^{1}H NMR (700 MHz, DMSO-d_6) δ 10.47 (s, 1H), 10.13 (s, 1H), 9.70 (s, 1H), 8.42 (d, J = 8.9 Hz, 1H), 8.25–8.23 (m, 2H), 8.04 (d, J = 2.6 Hz, 2H), 7.94 (d, J = 3.9 Hz, 2H), 7.71 (d, J = 8.6 Hz, 2H), 7.56–7.53 (m, 2H), 4.94 (s, 2H), 1.24 (s, 3H); MS (m/z): exact mass calcd for $C_{24}H_{19}N_5O_6$ $[M]^+$: 473.1. Found: 474.0. Anal. calcd for $C_{24}H_{19}N_5O_6$: C, 60.89; H, 4.05; N, 14.79. Found: C, 60.63; H, 3.56; N, 14.65.

4.1.2.5 N-(4-(2-(2-Hydroxybenzoyl)hydrazine-1-carbonyl) phenyl)-2-(3-methyl-2-oxoquinoxalin-1(2H)-yl)acetamide ***18.*** Yellow powder (yield 70%); mp: 255–257 °C; FT-IR (ν max, cm^{-1}): 3277, 3261, 2958, 1645, 1602, 1532; ^{1}H NMR (700 MHz, DMSO-d_6) δ 11.95 (s, 1H), 10.79–10.77 (m, 1H), 10.62 (s, 1H), 10.52 (d, J = 5.5 Hz, 1H), 7.81–7.80 (m, 2H), 7.72 (d, J = 8.7 Hz, 2H), 7.48–7.46 (m, 2H), 7.27 (d, J = 8.4 Hz, 1H), 7.17 (d, J = 7.6 Hz, 1H), 7.00–6.95 (m, 4H), 5.19 (s, 2H), 2.49 (d, J = 4.4 Hz, 3H); ^{13}C NMR (176 MHz, DMSO-d_6) δ 168.23, 167.57, 165.85, 159.79, 157.97, 154.85, 141.85, 134.64, 133.47, 132.47, 130.20, 129.28, 129.08, 128.74, 123.94, 122.15, 119.51, 118.99, 117.88, 115.21, 115.04, 68.33, 45.81, 21.59; MS (m/z): exact mass calcd for $C_{25}H_{21}N_5O_5$ $[M]^+$: 471.2. Found: 472.3. Anal. calcd for $C_{25}H_{21}N_5O_5$: C, 63.69; H, 4.49; N, 14.85. Found: C, 63.09; H, 4.41; N, 14.47.

4.2 Biological testing

4.2.1 ***In vitro*** **anti-proliferative activity.** MTT cytotoxicity assay[46–48,69,70] was utilized and it has been detailed in ESI.† In this test, all the synthesized compounds were evaluated for their anti-proliferative activities against MCF-7 and HepG-2 cell lines. The used cell lines were obtained from ATCC (American Type Culture Collection) *via* the Holding company for biological products and vaccines (VACSERA) (Cairo, Egypt).

4.2.2 ***In vitro*** **VEGFR-2 assay.** Human VEGFR-2 ELISA kit was used was carried out in this test following the reported method illustrated in ESI.†[71,72]

4.2.3 Cell cycle and apoptosis analysis. Flow cytometry technique was applied according to the reported methods described in ESI.†[50,73–75]

4.2.4 Western blot analysis. Western blot technique was performed for the most promising member against caspase-3, caspase-9, BAX, and Bcl-2 as described in ESI.†[76–78]

4.3 *In silico* studies

4.3.1 Docking studies. Docking studies were carried out against VEGFR-2 (PDB ID: 2OH$_4$) and CYP3A4 (PDB ID: 4D7D) using MOE 2014 and the results were visualized using Discovery studio 4.0 according to the procedure reported in ESI.†[79–82]

4.3.2 ADMET studies. ADMET descriptors were determined using Discovery studio 4.0 as according to the reported method[83–86] (ESI†).

4.3.3 Toxicity studies. Discovery studio 4.0 software was used to predict the toxicity potential of the synthesized compounds as reported in ESI.†[87,88]

4.3.4 DFT studies. Discovery studio 4.0 software was used to calculate the DFT parameter as reported in ESI.†

Conflicts of interest

There is no conflict of interest. Many thanks for Dr Mohamed R. Elnagar, Department of Pharmacology and Toxicology, Faculty of Pharmacy, Al-Azhar University, Cairo, Egypt for his valuable technical assistance.

Acknowledgements

The authors extend their appreciation to the Deanship of Scientific Research at King Saud University for funding this work through research group no (RG-1441-333).

References

1 G. H. Williams and K. Stoeber, *J. Pathol.*, 2012, **226**, 352–364.
2 K. Collins, T. Jacks and N. P. Pavletich, *Proc. Natl. Acad. Sci. U. S. A.*, 1997, **94**, 2776–2778.
3 A. Bennasroune, A. Gardin, D. Aunis, G. Crémel and P. Hubert, *Crit. Rev. Oncol. Hematol.*, 2004, **50**, 23–38.
4 M. K. Paul and A. K. Mukhopadhyay, *Int. J. Med. Sci.*, 2004, **1**, 101–115.
5 C. J. Peach, V. W. Mignone, M. A. Arruda, D. C. Alcobia, S. J. Hill, L. E. Kilpatrick and J. Woolard, *Int. J. Mol. Sci.*, 2018, **19**, 1264.
6 C. S. Abhinand, R. Raju, S. J. Soumya, P. S. Arya and P. R. Sudhakaran, *Cell Commun. Signaling*, 2016, **10**, 347–354.
7 G. Niu and X. Chen, *Curr. Drug Targets*, 2010, **11**, 1000–1017.
8 J. J. Bower, L. D. Vance, M. Psioda, S. L. Smith-Roe, D. A. Simpson, J. G. Ibrahim, K. A. Hoadley, C. M. Perou and W. K. Kaufmann, *npj Breast Cancer*, 2017, **3**, 9.
9 L. Huang, Z. Huang, Z. Bai, R. Xie, L. Sun and K. Lin, *Future Med. Chem.*, 2012, **4**, 1839–1852.
10 S. Tugues, S. Koch, L. Gualandi, X. Li and L. Claesson-Welsh, *Mol. Aspects Med.*, 2011, **32**, 88–111.
11 M. M. Maile, E. Y. T. Wong, D. Suzin, N. E. Birrer and R. T. Penson, in *Anti-Angiogenesis Drug Discovery and Development*, ed. R. Atta ur and M. I. Choudhary, Elsevier, 2014, pp. 191–215, DOI: 10.1016/B978-0-12-803963-2.50006-5.
12 G. M. Keating and A. Santoro, *Drugs*, 2009, **69**, 223–240.
13 S. M. Wilhelm, J. Dumas, L. Adnane, M. Lynch, C. A. Carter, G. Schütz, K. H. Thierauch and D. Zopf, *Int. J. Cancer*, 2011, **129**, 245–255.

14 K. Okamoto, M. Ikemori-Kawada, A. Jestel, K. von König, Y. Funahashi, T. Matsushima, A. Tsuruoka, A. Inoue and J. Matsui, *ACS Med. Chem. Lett.*, 2015, **6**, 89–94.
15 F. M. Yakes, J. Chen, J. Tan, K. Yamaguchi, Y. Shi, P. Yu, F. Qian, F. Chu, F. Bentzien, B. Cancilla, J. Orf, A. You, A. D. Laird, S. Engst, L. Lee, J. Lesch, Y. C. Chou and A. H. Joly, *Mol. Cancer Ther.*, 2011, **10**, 2298–2308.
16 A. De Luca and N. Normanno, *IDrugs*, 2010, **13**, 636–645.
17 E. Cabebe and H. Wakelee, *Drugs of today*, Barcelona, Spain, 2006, vol. 42, pp. 387–398.
18 Y. Liu and N. S. Gray, *Nat. Chem. Biol.*, 2006, **2**, 358–364.
19 M. M. Ghorab, M. S. Alsaid, A. M. Soliman and F. A. Ragab, *J. Enzyme Inhib. Med. Chem.*, 2017, **32**, 893–907.
20 M. Montana, V. Montero, O. Khoumeri and P. Vanelle, *Molecules*, 2020, **25**, 2784.
21 M. Montana, F. Mathias, T. Terme and P. Vanelle, *Eur. J. Med. Chem.*, 2019, **163**, 136–147.
22 E. M. Abbass, A. K. Khalil, M. M. Mohamed, I. H. Eissa and A. M. El-Naggar, *Bioorg. Chem.*, 2020, **104**, 104255.
23 M. A. Naylor, M. A. Stephens, J. Nolan, B. Sutton, J. H. Tocher, E. M. Fielden, G. E. Adams and I. J. Stratford, *Anti-Cancer Drug Des.*, 1993, **8**, 439–461.
24 T. H. Corbett, P. Lorusso, L. Demchick, C. Simpson, S. L. Pugh, K. White, J. Kushner, L. L. Polín, J. A. Meyer, J. Czarnecki, L. K. Heilbrun, J. P. Horwitz, J. L. Gross, C. H. Behrens, B. A. Harrison, R. J. Mcripley and G. L. Trainor, *Invest. New Drugs*, 2004, **16**, 129–139.
25 H. A. Mahdy, M. K. Ibrahim, A. M. Metwaly, A. Belal, A. B. M. Mehany, K. M. A. El-Gamal, A. El-Sharkawy, M. A. Elhendawy, M. M. Radwan, M. A. Elsohly and I. H. Eissa, *Bioorg. Chem.*, 2020, **94**, 103422.
26 A.-G. A. El-Helby, H. Sakr, I. H. Eissa, A. A. Al-Karmalawy and K. El-Adl, *Arch. Pharm.*, 2019, **352**, 1900178.
27 A.-G. A. El-Helby, H. Sakr, I. H. Eissa, H. Abulkhair, A. A. Al-Karmalawy and K. El-Adl, *Arch. Pharm.*, 2019, **352**, 1900113.
28 N. A. Alsaif, M. A. Dahab, M. M. Alanazi, A. J. Obaidullah, A. A. Al-Mehizia, M. M. Alanazi, S. Aldawas, H. A. Mahdy and H. Elkady, *Bioorg. Chem.*, 2021, **110**, 104807.
29 M. A. El-Zahabi, H. Sakr, K. El-Adl, M. Zayed, A. S. Abdelraheem, S. I. Eissa, H. Elkady and I. H. Eissa, *Bioorg. Chem.*, 2020, **104**, 104218.
30 S. A. El-Metwally, M. M. Abou-El-Regal, I. H. Eissa, A. B. Mehany, H. A. Mahdy, H. Elkady, A. Elwan and E. B. Elkaeed, *Bioorg. Chem.*, 2021, **112**, 104947.
31 A.-G. A. El-Helby, H. Sakr, R. R. Ayyad, H. A. Mahdy, M. M. Khalifa, A. Belal, M. Rashed, A. El-Sharkawy, A. M. Metwaly and M. A. Elhendawy, *Bioorg. Chem.*, 2020, **103**, 104233.
32 W. M. Eldehna, M. F. Abo-Ashour, A. Nocentini, P. Gratteri, I. H. Eissa, M. Fares, O. E. Ismael, H. A. Ghabbour, M. M. Elaasser and H. A. Abdel-Aziz, *Eur. J. Med. Chem.*, 2017, **139**, 250–262.
33 M. S. T. Nawaf, A. Alsaif, M. M. Alanazi, A. J. Obaidullah, A. A. Al-Mehizia, M. M. Alanazi, S. Aldawas, A. Elwan and H. Elkady, *J. Enzyme Inhib. Med. Chem.*, 2021, **36**, 1093–1114.
34 M. M. Alanazi, H. A. Mahdy, N. A. Alsaif, A. J. Obaidullah, H. M. Alkahtani, A. A. Al-Mehizia, S. M. Alsubaie, M. A. Dahab and I. H. Eissa, *Bioorg. Chem.*, 2021, **112**, 104949.
35 V. A. Machado, D. Peixoto, R. Costa, H. J. Froufe, R. C. Calhelha, R. M. Abreu, I. C. Ferreira, R. Soares and M. J. Queiroz, *Bioorg. Med. Chem.*, 2015, **23**, 6497–6509.
36 V. A. Machado, D. Peixoto, R. Costa, H. J. C. Froufe, R. C. Calhelha, R. M. V. Abreu, I. C. F. R. Ferreira, R. Soares and M.-J. R. P. Queiroz, *Bioorg. Med. Chem.*, 2015, **23**, 6497–6509.
37 J. Dietrich, C. Hulme and L. H. Hurley, *Bioorg. Med. Chem.*, 2010, **18**, 5738–5748.
38 G. W. H. Cheeseman, R. F. Cookson, *Chemistry of Heterocyclic Compounds*, ed. A. weissberger and E. C. Taylor, 1979, pp. 1–6, DOI: 10.1002/9780470187333.ch1.
39 D. Aparicio, O. A. Attanasi, P. Filippone, R. Ignacio, S. Lillini, F. Mantellini, F. Palacios and J. M. de Los Santos, *J. Org. Chem.*, 2006, **71**, 5897–5905.
40 M. Piltan, *J. Chem. Res.*, 2017, **41**, 712–714.
41 J. Gris, R. Glisoni, L. Fabian, B. Fernández and A. G. Moglioni, *Tetrahedron Lett.*, 2008, **49**, 1053–1056.
42 J. Cai, J. Zou, X. Pan and W. Zhang, *Tetrahedron Lett.*, 2008, **49**, 7386–7390.
43 Y. V. D. Nageswar, K. H. V. Reddy, K. Ramesh and S. N. Murthy, *Org. Prep. Proced. Int.*, 2013, **45**, 1–27.
44 M. M. Alanazi, H. A. Mahdy, N. A. Alsaif, A. J. Obiadullah, H. M. Alkahtani, A. A. Al-Mehizia, S. M. Alsubaie, M. A. Dahab and I. H. Eissa, *Bioorg. Chem.*, 2021, 104949.
45 M.-K. Ibrahim, A. A. Abd-Elrahman, R. R. Ayyad, K. El-Adl, A. M. Mansour and I. H. Eissa, *Bulletin of Faculty of Pharmacy*, Cairo University, 2013, vol. 51, pp. 101–111.
46 T. Mosmann, *J. Immunol. Methods*, 1983, **65**, 55–63.
47 F. Denizot and R. Lang, *J. Immunol. Methods*, 1986, **89**, 271–277.
48 M. Thabrew, R. D. Hughes and I. G. Mcfarlane, *J. Pharm. Pharmacol.*, 1997, **49**, 1132–1135.
49 P. O. Seglen, *Methods Cell Biol.*, 1976, **13**, 29–83.
50 J. Wang and M. J. Lenardo, *J. Cell Sci.*, 2000, **113**, 753–757.
51 J. Dietrich, C. Hulme and L. H. Hurley, *Bioorg. Med. Chem.*, 2010, **18**, 5738–5748.
52 X. Xia, E. G. Maliski, P. Gallant and D. Rogers, *J. Med. Chem.*, 2004, **47**, 4463–4470.
53 *BIOVIA, QSAR, ADMET and Predictive Toxicology*, https://www.3dsbiovia.com/products/collaborative-science/biovia-discovery-studio/qsar-admet-and-predictive-toxicology.html, accessed May 2020.
54 I. H. Eissa, A. M. El-Naggar, N. E. El-Sattar and A. S. Youssef, *Anti-Cancer Agents Med. Chem.*, 2018, **18**, 195–209.
55 C. Hansch, J. Björkroth and A. Leo, *J. Pharm. Sci.*, 1987, **76**, 663–687.
56 M. A. H. F. F. Utilizing, *J. Am. Chem. Soc.*, 1977, **99**, 8127–8134.
57 Y. Liang, Q.-S. Xu, H.-D. Li and D.-S. Cao, *Support Vector Machines and their Application in Chemistry and Biotechnology*, CRC Press, 2016.
58 H. C. Ansel, N. G. Popovich and L. V. Allen, *Pharmaceutical Dosage Forms and Drug Delivery Systems*, Williams & Wilkins, Baltimore, 1995.

59 E. Barim and F. Akman, *J. Mol. Struct.*, 2019, **1195**, 506–513.
60 G. Bitencourt-Ferreira and W. F. de Azevedo Junior, *Curr. Med. Chem.*, 2021, **28**(24), 4954–4971.
61 G. Náray-Szabó, *J. Mol. Recognit.*, 1993, **6**, 205–210.
62 R. Rohs, S. M. West, A. Sosinsky, P. Liu, R. S. Mann and B. Honig, *Nature*, 2009, **461**, 1248–1253.
63 A. J. McCoy, V. C. Epa and P. M. Colman, *J. Mol. Biol.*, 1997, **268**, 570–584.
64 M. M. Matin, M. S. Hasan, M. Uzzaman, M. M. H. Bhuiyan, S. M. Kibria, M. E. Hossain and M. H. Roshid, *J. Mol. Struct.*, 2020, **1222**, 128821.
65 I. H. Eissa, A.-G. A. El-Helby, H. A. Mahdy, M. M. Khalifa, H. A. Elnagar, A. B. Mehany, A. M. Metwaly, M. A. Elhendawy, M. M. Radwan and M. A. ElSohly, *Bioorg. Chem.*, 2020, 104380.
66 M. Ibrahim, M. Taghour, A. M. Metwaly, A. Belal, A. Mehany, M. Elhendawy, M. Radwan, A. Yassin, N. El-Deeb and E. Hafez, *Eur. J. Med. Chem.*, 2018, **155**, 117–134.
67 D. R. Romer, *J. Heterocycl. Chem.*, 2009, **46**, 317–319.
68 R. Sarges, H. R. Howard, R. G. Browne, L. A. Lebel, P. A. Seymour and B. K. Koe, *J. Med. Chem.*, 1990, **33**, 2240–2254.
69 S. T. Al-Rashood, A. R. Hamed, G. S. Hassan, H. M. Alkahtani, A. A. Almehizia, A. Alharbi, M. M. Al-Sanea and W. M. Eldehna, *J. Enzyme Inhib. Med. Chem.*, 2020, **35**, 831–839.
70 R. S. Ismail, S. M. Abou-Seri, W. M. Eldehna, N. S. Ismail, S. M. Elgazwi, H. A. Ghabbour, M. S. Ahmed, F. T. Halaweish and D. A. Abou El Ella, *Eur. J. Med. Chem.*, 2018, **155**, 782–796.
71 S. M. Abou-Seri, W. M. Eldehna, M. M. Ali and D. A. Abou El Ella, *Eur. J. Med. Chem.*, 2016, **107**, 165–179.
72 I. H. Eissa, A.-G. A. El-Helby, H. A. Mahdy, M. M. Khalifa, H. A. Elnagar, A. B. Mehany, A. M. Metwaly, M. A. Elhendawy, M. M. Radwan and M. A. ElSohly, *Bioorg. Chem.*, 2020, **105**, 104380.
73 W. M. Eldehna, G. S. Hassan, S. T. Al-Rashood, T. Al-Warhi, A. E. Altyar, H. M. Alkahtani, A. A. Almehizia and H. A. Abdel-Aziz, *J. Enzyme Inhib. Med. Chem.*, 2019, **34**, 322–332.
74 K. K.-W. Lo, T. K.-M. Lee, J. S.-Y. Lau, W.-L. Poon and S.-H. Cheng, *Inorg. Chem.*, 2008, **47**, 200–208.
75 A. Sabt, O. M. Abdelhafez, R. S. El-Haggar, H. M. Madkour, W. M. Eldehna, E. E.-D. A. El-Khrisy, M. A. Abdel-Rahman and L. A. Rashed, *J. Enzyme Inhib. Med. Chem.*, 2018, **33**, 1095–1107.
76 A. Balah, O. Ezzat and E.-S. Akool, *Int. Immunopharmacol.*, 2018, **65**, 493–502.
77 N. M. Aborehab, M. R. Elnagar and N. E. Waly, *J. Biochem. Mol. Toxicol.*, 2020, e22638.
78 M. R. Elnagar, A. B. Walls, G. K. Helal, F. M. Hamada, M. S. Thomsen and A. A. Jensen, *Eur. J. Pharmacol.*, 2018, **826**, 106–113.
79 A. G. A. El-Helby, R. R. Ayyad, H. M. Sakr, A. S. Abdelrahim, K. El-Adl, F. S. Sherbiny, I. H. Eissa and M. M. Khalifa, *J. Mol. Struct.*, 2017, **1130**, 333–351.
80 A. A. Nasser, I. H. Eissa, M. R. Oun, M. A. El-Zahabi, M. S. Taghour, A. Belal, A. M. Saleh, A. B. Mehany, H. Luesch and A. E. Mostafa, *Org. Biomol. Chem.*, 2020, **18**, 7608–7634.
81 A. M. El-Naggar, I. H. Eissa, A. Belal and A. A. El-Sayed, *RSC Adv.*, 2020, **10**, 2791–2811.
82 M. Hagras, M. A. El Deeb, H. S. Elzahabi, E. B. Elkaeed, A. B. Mehany and I. H. Eissa, *J. Enzyme Inhib. Med. Chem.*, 2021, **36**, 640–658.
83 M. A. El-Zahabi, E. R. Elbendary, F. H. Bamanie, M. F. Radwan, S. A. Ghareib and I. H. Eissa, *Bioorg. Chem.*, 2019, **91**, 103115.
84 M. K. Ibrahim, I. H. Eissa, M. S. Alesawy, A. M. Metwaly, M. M. Radwan and M. A. ElSohly, *Bioorg. Med. Chem.*, 2017, **25**, 4723–4744.
85 A. El-Demerdash, A. M. Metwaly, A. Hassan, A. El-Aziz, T. Mohamed, E. B. Elkaeed, I. H. Eissa, R. K. Arafa and J. D. Stockand, *Biomolecules*, 2021, **11**, 460.
86 K. M. El-Gamal, A. M. El-Morsy, A. M. Saad, I. H. Eissa and M. Alswah, *J. Mol. Struct.*, 2018, **1166**, 15–33.
87 I. H. Eissa, M. A. Dahab, M. K. Ibrahim, N. A. Alsaif, A. Alanazi, S. I. Eissa, A. Belal and A. M. Beauchemin, *Bioorg. Chem.*, 2021, 104965.
88 M. M. Alanazi, I. H. Eissa, N. A. Alsaif, A. J. Obaidullah, W. A. Alanazi, A. F. Alasmari, H. Albassam, H. Elkady and A. Elwan, *J. Enzyme Inhib. Med. Chem.*, 2021, **36**, 1760–1782.